Research Paper
Journal of Aerospace System Engineering
Vol.15, No.6, pp.10-18 (2021)

EISSN 2508-7150
http://dx.doi.org/10.20910/JASE.2021.15.6.10

Numerical Study of Ablation Phenomena of Flame Deflector

Wonseok Lee†, Yeongrok Yang, Sangmok Shin, Jaecheol Shin

Missile Research Institute - 9th Directorate, Agency for Defense Development, Korea

Abstract

A flame deflector prevents a launch system from thermal damage by deflecting the exhaust flame of the launch vehicle. During the deflection of the flame, the flame deflector is subjected to a high-temperature and high-pressure flow, which results in thermal ablation damage at the surface. Predicting this ablation damage is an essential requirement to ensure a reliable design. This paper introduces a numerical method for predicting the ablation damage phenomena based on a one-way fluid–structure interaction (FSI) analysis. In the proposed procedure, the temperature and convective heat transfer coefficient of the exhaust flame are calculated using a fluid dynamics analysis, and then the ablation is calculated using a finite element analysis (FEA) based on the user-subroutine UMESHMOTION and Arbitrary Lagrangian–Eulerian (ALE) adaptive mesh technique in ABAQUS. The result of such an analysis was verified by comparison to the ablation test result for a flame deflector.

Key Words: Flame Deflector, Ablation, One-way Fluid–Structure Analysis, Fluid Dynamics Analysis, Finite Element Analysis

Notations

$\dot{Q}$ **: Heat flux**

T_r **: Temperature of exhaust flame**

T_w **: Temperature of the flame deflector wall**

h **: Convective heat transfer coefficient**

ρ **: Density**

c **: Specific heat**

k **: Thermal conductivity**

$\triangle t$ **: Time increment in simulation**

L **: Mesh length**

y^N **: Coordinates of the node in the vertical direction**

T^N **: Temperature of node**

v **: Speed of the ablation surface movement**

p **: Increment number**

A **: Directional cosine tensor**

r **: Ablation rate**

η_m **: Melting temperature surface in the normal coordinates**

1. Introduction

In the hot launch method for a projectile, the thrust of the projectile is produced by the heat of the flames of the booster, and at the moment of the projectile's initial take-off, the generated exhaust flame has a very high temperature and velocity. Because the generated exhaust flame may be reflected from the ground, which can cause the launch vehicle and launch system to be engulfed in flames in an instant, it is crucial that these be equipped with a flame deflector to protect the launch system from these high-temperature/high-pressure flames [1].

Received: Jul. 09, 2021 Revised: Sep. 13, 2021 Accepted: Sep. 15, 2021
† Corresponding Author
Tel: +82-42-821-4213, E-mail: leews21@gmail.com

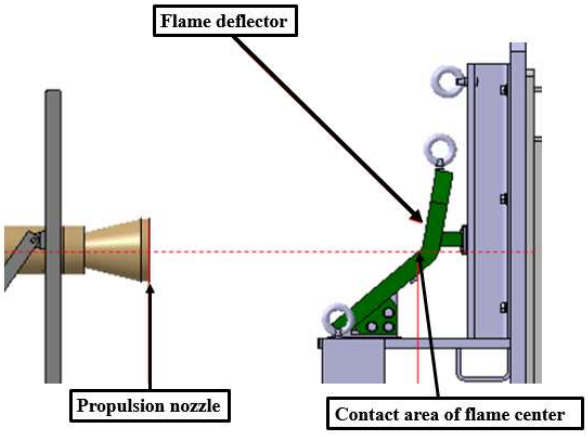

Fig. 1 Schematic of launcher flame deflector

Fig. 1 presents a schematic of a flame deflector. The flame deflector deflects the exhaust flame generated from the propulsion system of the launch vehicle to the rear of the launch system using an inclined surface, while simultaneously preventing the flame from infiltrating the launch system. In this process, the metal flame deflector is directly exposed to the high-temperature and high-pressure exhaust flame. Although the duration of the burn is short, this leads to the mechanical or chemical ablation of the surface of the flame deflector. If the surface shape is changed by this ablation, this will not only affect the fluid dynamics of the flames but also cause a structural degradation problem with the flame deflector with repeated use. Therefore, in order to implement a reliable design for the flame deflector, it is imperative to predict the ablation phenomenon and ablation depth on the surface. However, it is difficult to consider all of the complex boundary conditions for the fluid-heat-structure at the same time. Furthermore, because of the complex physical behaviors on the surface, using a numerical analysis to predict the ablation phenomenon is complicated and difficult in practice.

In this study, we employed a one-way fluid–structure interaction (FSI) analysis with the application of the UMESHMOTION subroutine and Arbitrary Lagrangian–Eulerian (ALE) adaptive meshing algorithm to develop a method for predicting the ablation phenomenon and ablation depth of a flame deflecting plate. A one-way FSI analysis is a generalized method used for blade analyses that was proposed by Kim et al. [2–4] and is very useful for evaluating the safety of a thermal structure without the need for continuous iterative calculations. However, this method has the disadvantage that it cannot perform calculations on the surface ablation phenomenon that may arise during a hot-gas combustion process. In order to address this limitation and enable the analysis of the surface ablation phenomenon that occurs when the surface reaches the ablation temperature in a one-way FSI analysis, this study applied the UMESHMOTION subroutine and ALE adaptive meshing algorithm in the commercial code ABAQUS [5–10]. This method was capable of calculating the ablation phenomenon that could occur in the combustion process. The results of a numerical analysis were compared with those of an ablation test of a flame detector, which verified the validity and effectiveness of the analysis method developed in this study.

2. Methods

2.1 Ablation test of flame deflector

The experimental setup for the ablation test of the flame deflector, which was the subject of the analysis, is presented in Fig. 2, and Fig. 3 shows a picture of the test itself.

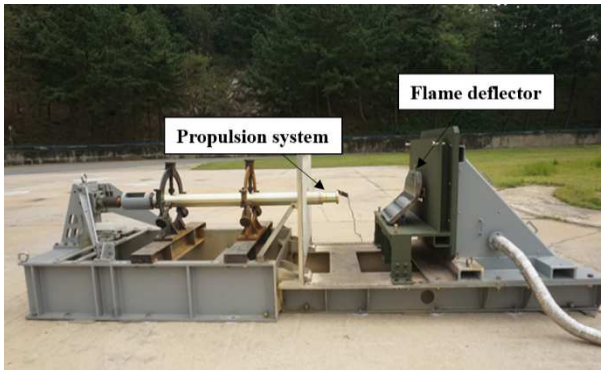

Fig. 2 Experimental setup of ablation test

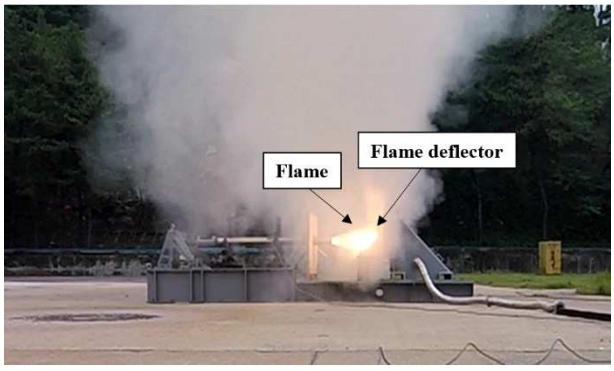

Fig. 3 Picture of ablation test

The flame generated by the propulsion system was in direct contact with the flame deflecting plate, which deflected it, as seen in the figure. In this process, the flame deflecting plate was subjected to a thermal load from the high-temperature and high-pressure flames, and surface ablation occurred.

Fig. 4 Ablation test result

Figure 4 shows the ablation test results, including the ablation shape and point of maximum ablation of the flame deflector. The maximum ablation was observed at the center, where the thermal load of the exhaust flame was concentrated, and the ablation depth was measured at approximately 2.53 mm. The ablation shape and ablation depth were analyzed through simulations.

2.2 Computational fluid analysis

The governing equation for the convective heat transfer of the flame deflector by the exhaust flame of the launch vehicle can be expressed as follows:

$$\dot{Q} = h(T_r - T_w) \quad , \tag{1}$$

where $\dot{Q}$ represents the heat flux passing through the flame deflector wall (W/m^2), T_r is the temperature of the exhaust flame, T_w is the temperature at the flame deflector wall, and $h(W/m^2K)$ is the convective heat transfer coefficient.

2.2.1 Boundary conditions

This study used CFD-FASTRAN, which is a commercial computational fluid dynamics (CFD) code from ESI. A steady state was assumed, the compressible Navier–Stokes equation was used as the governing equation, and a 3D CFD simulation was performed. The Baldwin–Lomax model was used for the turbulence model. Sutherland's law was applied for the viscosity model, and a cell-based Van Leer flux vector splitting (FVS) scheme was used as the numerical technique. Wall boundary conditions were used for the flame deflector, where the convective heat transfer coefficient at the wall boundary was derived by applying the wall boundary conditions at a temperature of 1000 K [3]. The temperature and pressure conditions at the nozzle inlet were 3550 K and 990 psi, respectively, and atmospheric pressure was applied for the outlet conditions.

2.2.2 Results of analysis

The results of the numerical analysis are shown in Figs. 5–7, where Fig. 5 presents the Mach number distribution, Fig. 6 shows the temperature distribution, and Fig. 7 shows the pressure distribution. As can be seen from Figs. 6 and 7, there was no direct flame introduced onto the bottom surface of the flame deflecting plate. The pressure and temperature acting on the flame deflecting plate were found to be the highest near the center point of the launch vehicle. The maximum pressure was approximately 16 bar, and the maximum temperature was approximately 3500 K.

Figure 8 shows the results of a CFD analysis of the heat flux distribution. The model was a 1/2 symmetric model, and the maximum heat flux near the center of the flame deflecting plate was calculated to be 4.66 × 107 W/m^2. Based on this result, the maximum convective heat transfer coefficient was 1.86 × 104 W/m^2·K near the center point, and the derived convective heat transfer coefficient and temperature of the exhaust flame were applied as input conditions for the heat transfer analysis.

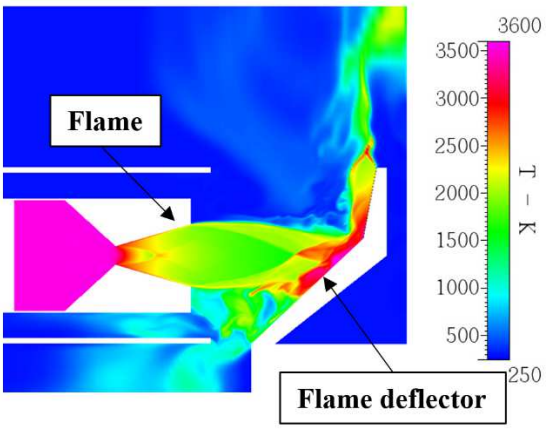

Fig. 5 Mach number distribution

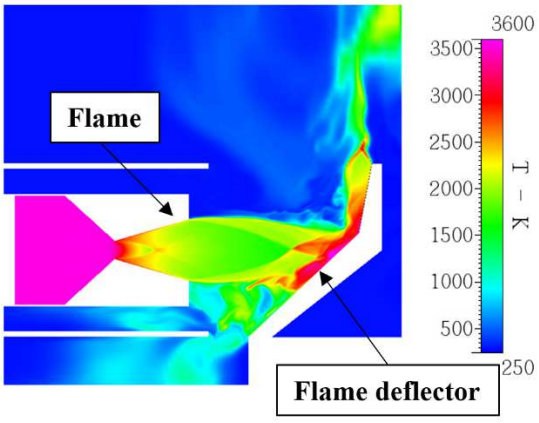

Fig. 6 Temperature distribution

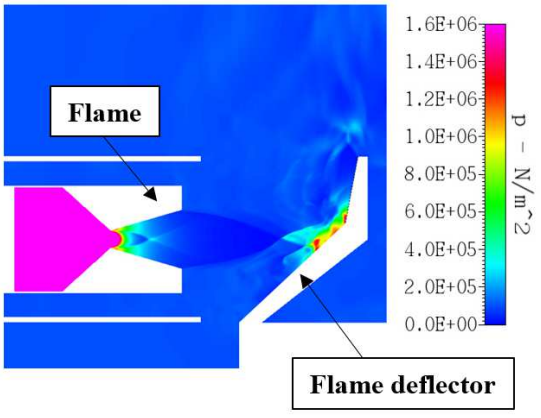

Fig. 7 Pressure distribution

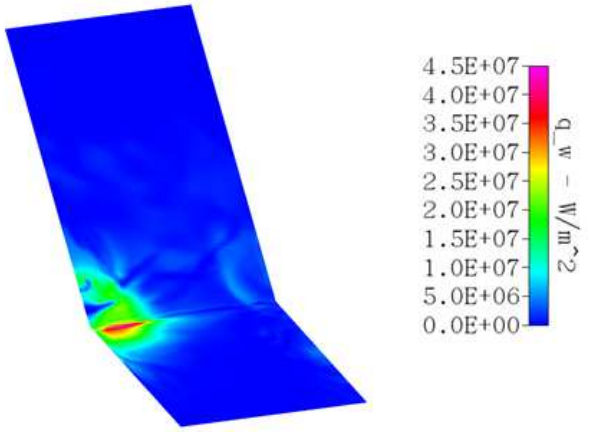

Fig. 8 Heat flux distribution

2.3 Heat transfer and ablation interaction analysis

The governing equation for the heat conduction inside the flame deflector can be expressed as follows:

$$\rho c(T)\frac{\partial T}{\partial t} = \nabla \cdot (k(T)\nabla T) \quad , \tag{2}$$

where ρ denotes the density, c is the specific heat, and k is the thermal conductivity.

2.3.1 Numerical analysis model

The commercial analysis program ABAQUS was used to develop the finite element model (FE model) used in the analyses of the heat transfer and ablation interactions, as illustrated in Fig. 9. In order to reduce the simulation time, the model was simplified by considering it to be symmetrical with respect to the center axis. Because the concentration of the ablation phenomena was expected in the center area of the flame deflection part, a dense mesh composition was used in the center area, with the mesh size increasing in the area further from the center to improve the computation speed. To accurately calculate the ablation phenomenon on the flame deflecting plate surface in the thickness direction, a dense mesh composition was also used in the thickness direction.

For the FE model used in the analyses of the heat transfer and ablation interactions, the mesh structure was constructed with hexagonal elements (C3D8T, three-dimensional eight-node elements). The number of elements was 173,214, and the number of nodes was 153,432 in total.

To ensure an accurate analysis, the mesh length and time increment in the simulation were adjusted to satisfy Eq. (3) [11].

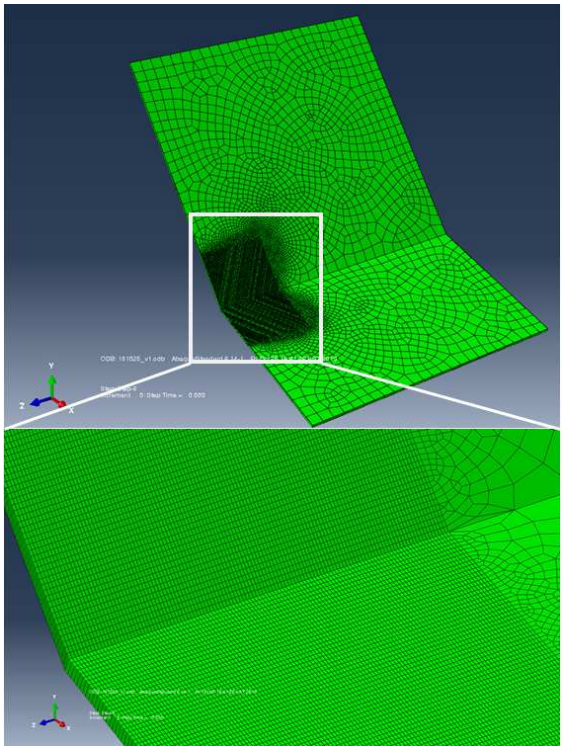

Fig. 9 Analysis model of launcher flame deflector

$$\triangle t > \frac{\rho L^2 c}{6k} \quad (3)$$

Here, $\triangle t$ denotes the time increment in the simulation, and L represents the mesh size.

2.3.2 Boundary conditions

Figure 10 shows the mapping result for the convective heat transfer coefficient and flame temperature derived from the CFD analysis as boundary conditions for the ablation analysis model, where the parts indicated in yellow highlights represent the mapped boundary conditions

For the solver type, the thermo-mechanical coupling (TMC) method was applied, and the initial temperature of the flame deflector was set to 20 ℃. For boundary conditions, U1, U2, and U3 = 0 were applied to the top part. For the simulation conditions, the one-way FSI analysis method [1–2] was applied, in which the thermal load was applied by mapping the convective heat transfer coefficient and flame temperature calculated through the CFD analysis to the heat transfer-ablation analysis model. The one-way FSI analysis method is applicable in cases where the effect on the flow is small because the displacement caused by the thermal load is not significant in the analysis subject, and this method does not require continuous iterative calculations.

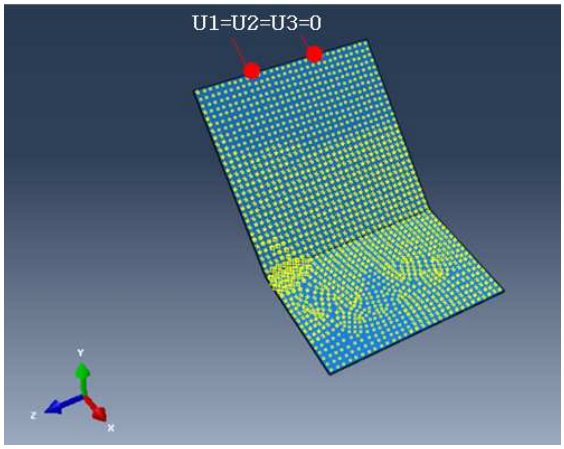

Fig. 10 Boundary condition for ablation analysis

Because the burning time lasted for 2 s, the convective and conductive heat transfer lasted for 2 s, as shown in the thermal load profile of Fig. 11, and the natural convection condition of 10 W/m^2·K was applied to the rear side of the flame deflecting plate.

Table 1 outlines the temperature-dependant material properties of the flame deflector.

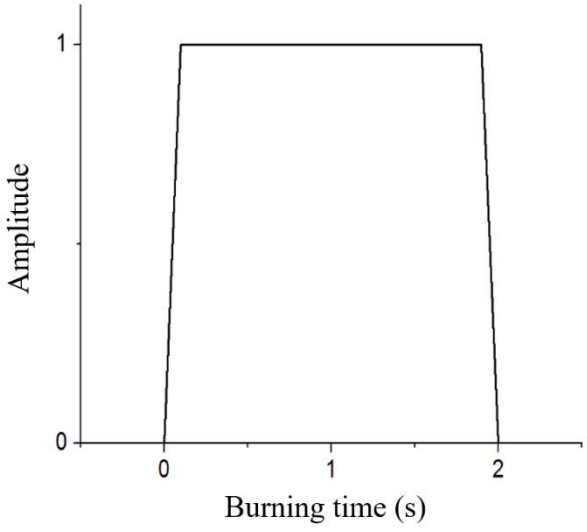

Fig. 11 Thermal load profile

Table 1 Temperature-dependent material properties

Temperature (K)	Density (kg/m^3)	Thermal conductivity (W/m [T])	Heat capacity (J/kg·K)
273	7880	60	480
373	7880	50	500
473	7880	45	520
673	7760	38	650
873	7600	30	750
1073	7520	25	1000
1473	7300	28	1400
1573	7250	37	1600

The local ablation phenomenon on the surface of the flame deflector involved chemical or mechanical ablation. Chemical ablation is defined as a phenomenon in which the high temperature of a flame causes the surface to melt and continue to increase in temperature, which leads to boiling and eventually to the loss or consumption of the material on the surface. Mechanical ablation is defined as a phenomenon in which loss occurs on the surface of the melted metal in the same way as when struck by a solid object as a result of physical vibration phenomena such as the forces of the high-speed exhaust fluid. Based on the results of a combustion test of the nozzle throat of a rocket engine, which is similar to the ablation phenomenon that occurs with a flame deflector, as well as scanning electron microscopy (SEM) results [12], the ablation surface was found to undergo greater delamination by mechanical collision than by chemical ablation. The surface ablation mechanism on the surface of the flame deflector was also considered to be dominated by the mechanical ablation caused by the force of the exhaust fluid on the molten metal surface. Thus, the melting point of the material of the flame deflector surface was set as the criterion for the occurrence of the oblation phenomenon. The material of the flame deflecting plate was carbon steel (carbon content 0.2%), and its melting point temperature was 1745 K.

A user-subroutine was applied in the commercial ABAQUS code to implement the ablation phenomenon. The ablation analysis method was programmed in the UMESHMOTION subroutine, and the ALE adaptive meshing algorithm was applied, in which an adaptive rearrangement of the meshing was carried out in the ablation region to prevent simulation errors due to excessive deformation, facilitate the convergence, and increase the accuracy of the numerical analysis [5–10]. A flow chart showing the ablation analysis process is presented in Fig. 12.

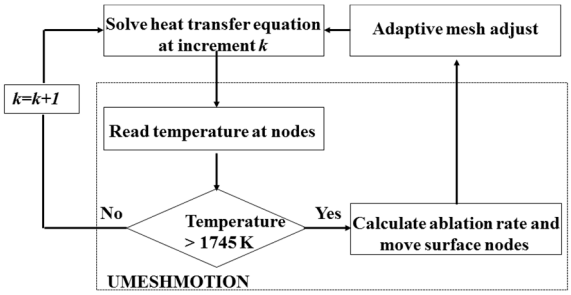

Fig. 12 Flow chart of UMESHMOTION+ALE method

After performing the heat transfer analysis of the flame deflecting plate using the convective heat transfer and temperature of the exhaust flame, it was determined from the results whether the calculated temperature for each node was 1745 K or higher, which was the melting point. When the temperature at a node of the surface was higher than the melting point, the node was moved by the calculated ablation rate, and the mesh that contained the moved node was rearranged by the remeshing function of ALE.

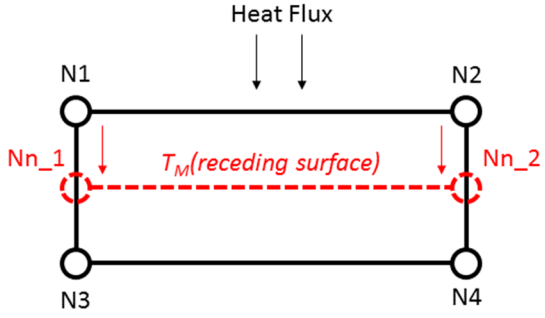

Fig. 13 Principle of node motion

Figure 13 shows the mesh motion on the ablation surface from the UMESHMOTION subroutine. The surface at *N1* and *N2*, which were nodes 1 and 2 where the temperature was higher than the melting point as a result of the convective heat transfer, receded to the surface at *Nn_1* and *Nn_2, the surface of the melting temperature* (T_m, red dotted line), and the moved meshes underwent remeshing by the ALE algorithm. The elements of the nodes that reached the melting point temperature or higher retreated to the surface of the melting point through the repeated receding of the mesh. *Nn_1* and *Nn_2*, which were the node coordinates of receding surface T_m, were shape functions based on Lagrange polynomials and can be defined using the following equations [13].

$$Nn\_1 = \frac{1}{2}((1-\eta_m) \cdot y^{N1} + (1+\eta_m) \cdot y^{N3}) \quad (4)$$

$$Nn\_2 = \frac{1}{2}((1-\eta_m) \cdot y^{N2} + (1+\eta_m) \cdot y^{N4}) \tag{5}$$

Here, y denotes the vertical coordinates of node N1–4, and η_m represents the melting temperature surface in the normal coordinates with ξ and η as the axes, which is where the surface with a temperature at the melting point or higher retreats. This can be defined as follows:

$$\eta_m = \frac{T^{N1} + T^{N3} - 2T_m}{T^{N1} - T^{N3}} \tag{6}$$

where T is the temperature of each node (N1–4), and T_m is the temperature at the melting point.

Equations (7) and (8) represent the movement speed and displacement of the ablation surface, respectively [5].

$$\begin{bmatrix} v_x^{p+1} \\ v_y^{p+1} \end{bmatrix} = \begin{bmatrix} v_x^{p} \\ v_y^{p} \end{bmatrix} - A \cdot \begin{bmatrix} r_x \\ r_y \end{bmatrix} \tag{7}$$

$$\begin{bmatrix} x^{p+1} \\ y^{p+1} \end{bmatrix} = \begin{bmatrix} v_x^{p+1} \\ v_y^{p+1} \end{bmatrix} \cdot \triangle t \tag{8}$$

Here, v_x and v_y are the movement speeds of the ablation surface in the x and y directions, respectively, which correspond to ULOCAL in the UMESHMOTION subroutine. x and y are the displacements of the ablation surface, p is the increment number, and A is the directional cosine tensor corresponding to ALOCAL in the UMESHMOTION subroutine. r_x and r_y are the ablation rates in the directions of x and y, respectively.

The UMESHMOTION subroutine and remeshing method of the ALE algorithm have the advantage of not having to perform iterative calculation processes and reenter the thermal conditions for each cycle of the simulation because with the application of the thermal input conditions, the surface nodes are not deleted but retained as a result of the movement of the mesh. For the ablation analysis of the flame deflector, a transient analysis was performed using ABAQUS/IMPLICIT, which made it possible to observe the ablation phenomenon over time.

2.3.3 Analysis result

The temperature distribution and ablation on the flame deflector surface were observed for a flame burning time of 2 s. Figure 14 shows the results at 0 s and 0.54 s of the burning time.

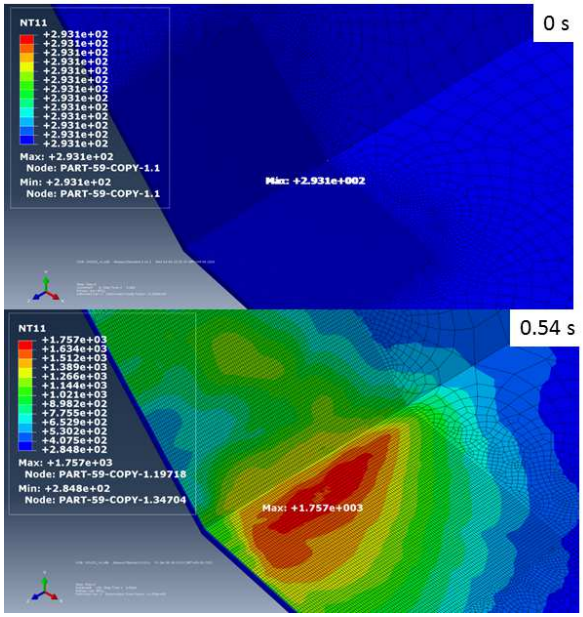

Fig. 14 Temperature distributions of ablation analysis at 0 and 0.54 s

In the temperature distribution figure, it can be seen that the rise in temperature was concentrated in the center part of the flame. At 0.54 s, the temperature of the flame deflecting plate showed a gradual increase because of the convective heat transfer, and the maximum surface temperature of 1757 K was observed at the center of the flame. Thus, it can be seen that the ablation temperature exceeded 1745 K, the melting temperature. Examining the result at 0.54 s in detail, local ablation can be observed in the center where the temperature exceeded the melting point.

Figure 15 shows the shape change results over time from 0.54 s when the ablation started to 2.1 s. At 0.54 s, the surface temperature exceeded the melting point of 1745 K, and local ablation started. Then, at 0.94 s and 1.44 s, the region exceeding the melting point gradually expanded, and the ablation continued in the direction of the thickness. At 2.1 s, after the flame combustion was finished, the surface temperature decreased to the melting point or lower, indicating that the ablation stopped. From this result, it can be seen that during the ablation process from 0.54 s to 2.1 s, the maximum surface temperature did not exceed 1757 K, the melting point, indicating that the ablation phenomenon could be properly represented with the movement of the mesh.

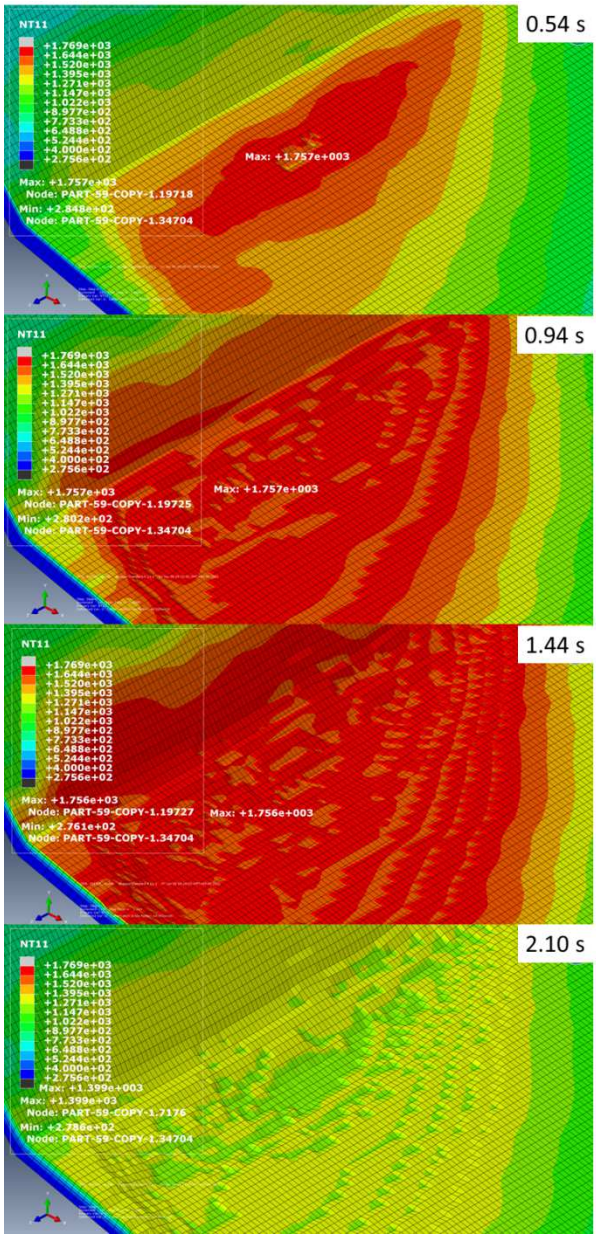

Fig. 15 Shape change results at 0.54 s, 0.94 s, 1.44 s, and 2.10 s

The ablation results before and after flame combustion are presented in Fig. 16, which shows that the maximum ablation depth was 3.55 mm at the flame center.

A comparison of the ablation distributions found in the test and numerical analysis is presented in Fig. 17. The simulation results are for the 1/2 axial symmetry model and show highly similar ablation patterns compared to the 1/2 axial symmetry results of the ablation test. A comparison of the ablation depths showed that the ablation depth obtained from the test was 2.53 mm, and that obtained from the numerical analysis was 3.55 mm, which was a difference of 1.02 mm. In order to reduce the errors between the results of the analysis and test in the future, we aim to improve the accuracy by additionally considering the endothermic reaction energy and oxidation heat generated during the ablation process.

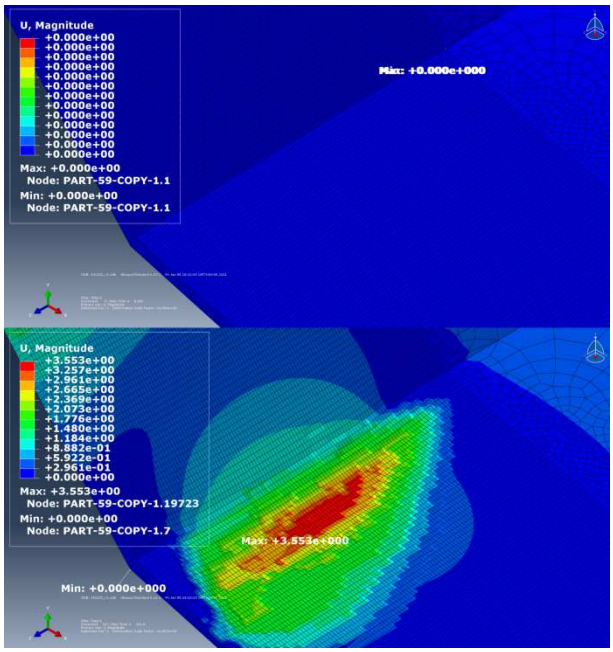

Fig. 16 Ablation depth results

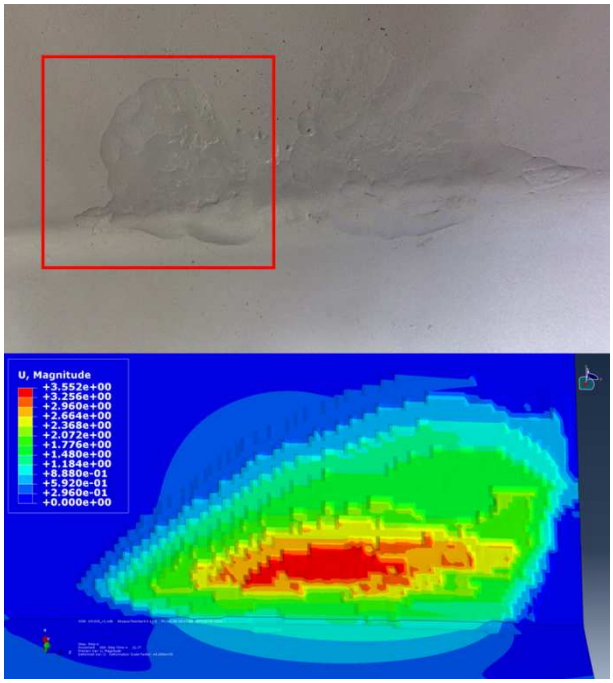

Fig. 17 Comparison of ablation phenomena found in test and analysis

3. Conclusion

In this study, in order to predict the ablation phenomenon and ablation depth on the surface of a flame deflector by a thermal reaction, the UMESHMOTION subroutine and ALE remeshing algorithm were applied to a one-way FSI analysis to conduct a CFD analysis. The process of the numerical analysis is outlined as follows.

(1) The temperature distribution transmitted to the surface of the flame deflector by the exhaust flame and the convective heat transfer coefficient were derived through the CFD analysis, and the results were applied as input conditions in the heat transfer analysis.
(2) The surface ablation phenomenon that occurred when the surface temperature reached the ablation temperature as a result of the heat transfer was analyzed by applying the UMESHMOTION subroutine and ALE remeshing algorithm to the commercial code ABAQUS.
(3) Based on the above analysis results, the ablation patterns and ablation depth on the surface of the flame deflector were finally derived.

The above numerical analysis results were compared with the results of an ablation test of an actual flame deflector. Significant similarity was observed for the ablation patterns and ablation depths in the test results and analysis results. Therefore, the validity of the proposed method for flame ablation analysis was verified in this study. The proposed method is expected to provide a basis for the prediction and applications of the ablation distribution and ablation depth of a flame deflector in the development of launch systems. In the future, we aim to improve the accuracy of the method with the additional consideration of the endothermic reaction energy and oxidation heat generated during the ablation process.

References

[1] H. Oh, S. Kang, D. Kim, J. Lee, H. Um, and H. Huh, “Conceptual design of KSLV-II launch complex flame deflector,” *2014 KSPE Spring Conference*, pp. 405–410, 2014.
[2] Y. G. Kim and K. C. Kim, “FSI analysis on wind turbine blade,” *Trans. Korean Soc. Mech. Eng. B*, pp. 2368–2371, 2007.
[3] J. B. Ko, M. K. Seo, K. H. Lee, B. K. Beak, and S. H. Cho, “A study on the 1-way FSI analysis for shutter of side jet thruster,” *Trans. Korean Soc. Mech. Eng. A*, vol. 38, no. 12, pp. 1359–1365, 2014.
[4] M. Kang, D. Park, and S. Lee., “The study of aerodynamic about high-speed projectiles using fluid structure interaction analysis,” *J. Aerosp. Syst. Eng*., vol. 6, no. 4, pp. 12–17, 2012.
[5] Y. Wang, N. Shen, G. K. Befekadu, and C. L. Pasiliao, “Modeling pulsed laser ablation of aluminum with finite element analysis considering material moving front,” *Int. J. Heat. Mass. Tran*., 113, 1246-1253, 2017.
[6] H. Cheon, et al., “Prediction of wear profile of tire using steady-state rolling analysis method,” *KSAE 2009 Annual conference*, pp. 1668–1671, Nov, 2009.
[7] K. Y. Hwang and J. Y. Bae, “Thermal response modeling of thermal protection materials and application trends of commercial codes for flow-thermal-structural analysis,” *J. Korean Soc. Propul. Eng.*, vol. 23, no. 6, pp. 59–71, 2019.
[8] Y. Ro, S. Seok, and S. Jeong, “An evaluation on thermal-structural behavior of nozzle assembly during burning time,*” J. Korean Soc. Propul. Eng.*, vol. 22, no. 4, pp. 36–43, 2018.
[9] C. Lee, et al., “FSbi simulation for solid propellant rocket interior with flame propagation delay and secondary burning,” *KIMST Annual Conference Proceedings*, pp. 1575–1576, July, 2014.
[10] M. Lee, “Development of 3-Dim FEM multi-material hydrocode,” *J. Korea Inst. Mil. Sci. Technol*., vol. 11, no. 5, pp. 116–123, 2008.
[11] H. R. Thomas and Z. Zhou, “Minimum time-step size for diffusion problem in FEM analysis,” *Int. J. Number. Meth. Eng.*, vol. 40, pp. 3865–3880, 1997.
[12] E. H. Zhang, Z. B. Kim, and H. J. Joo, “Ablative mechanism of SiC coated carbon/carbon composites with ratio of oxygen to fuel at combustion test,” *J. Korean Ind. Eng. Chem.*, vol. 18, no. 3, pp. 227–233, 2007.
[13] B. Kawecki and P. Jerzy, “Numerical results quality in dependence on ABAQUS plane stress elements type in big displacements compression test,” *Appl. Comp. Sci.*, vol. 13, no. 4, pp. 56–64, 2017.